

RESEARCH ARTICLE

AEROSOL FORMATION

Role of iodine oxoacids in atmospheric aerosol nucleation

Xu-Cheng He^{1*}, Yee Jun Tham¹, Lubna Dada¹, Mingyi Wang², Henning Finkenzeller³, Dominik Stolzenburg^{4,1}, Siddharth Iyer⁵, Mario Simon⁶, Andreas Kürten⁶, Jiali Shen¹, Birte Rörup¹, Matti Rissanen⁵, Siegfried Schobesberger⁷, Rima Baalbaki¹, Dongyu S. Wang⁸, Theodore K. Koenig³, Tuija Jokinen¹, Nina Sarnela¹, Lisa J. Beck¹, João Almeida⁹, Stavros Amanatidis¹⁰, António Amorim¹¹, Farnoush Aataei¹², Andrea Baccarini⁸, Barbara Bertozzi¹³, Federico Bianchi¹, Sophia Brilke⁴, Lucia Caudillo⁶, Dexian Chen², Randall Chiu³, Biwu Chu¹, António Dias¹¹, Aijun Ding^{14,15}, Josef Dommen⁸, Jonathan Duplissy^{1,16}, Imad El Haddad⁸, Loïc Gonzalez Carracedo⁴, Manuel Granzin⁶, Armin Hansel^{17,18}, Martin Heinritzi⁶, Victoria Hofbauer², Heikki Junninen^{19,1}, Juha Kangasluoma¹, Deniz Kemppainen¹, Changhyuk Kim^{10,20}, Weimeng Kong¹⁰, Jordan E. Krechmer²¹, Aleksander Kvashin²², Totti Laitinen¹, Houssni Lamkaddam⁸, Chuan Ping Lee⁸, Katrianne Lehtipalo^{1,23}, Markus Leiminger^{17,18}, Zijun Li⁷, Vladimir Makhmutov²², Hanna E. Manninen⁹, Guillaume Marie⁸, Ruby Marten⁸, Serge Mathot⁹, Roy L. Mauldin²⁴, Bernhard Mentler¹⁷, Ottmar Möhler¹³, Tatjana Müller⁶, Wei Nie^{14,15}, Antti Onnela⁹, Tuukka Petäjä¹, Joschka Pfeifer⁹, Maxim Philippov²², Ananth Ranjithkumar²⁵, Alfonso Saiz-Lopez²⁶, Imre Salma²⁷, Wiebke Scholz^{17,18}, Simone Schuchmann²⁸, Benjamin Schulze¹⁰, Gerhard Steiner¹⁷, Yuri Stozhkov²², Christian Tauber⁴, António Tomé²⁹, Roseline C. Thakur¹, Olli Väistänen⁷, Miguel Vazquez-Pufleau⁴, Andrea C. Wagner^{3,6}, Yonghong Wang¹, Stefan K. Weber⁹, Paul M. Winkler⁴, Yusheng Wu¹, Mao Xiao⁸, Chao Yan¹, Qing Ye², Arttu Ylsirniö⁷, Marcel Zauner-Wieczorek⁶, Qiaozhi Zha¹, Putian Zhou¹, Richard C. Flagan¹⁰, Joachim Curtius⁶, Urs Baltensperger⁸, Markku Kulmala^{1,14,16,30}, Veli-Matti Kerminen¹, Theo Kurtén³¹, Neil M. Donahue^{2,32,33,34}, Rainer Volkamer³, Jasper Kirkby^{9,6,*}, Douglas R. Worsnop^{1,21}, Mikko Sipila^{1*}

Iodic acid (HIO_3) is known to form aerosol particles in coastal marine regions, but predicted nucleation and growth rates are lacking. Using the CERN CLOUD (Cosmics Leaving Outdoor Droplets) chamber, we find that the nucleation rates of HIO_3 particles are rapid, even exceeding sulfuric acid–ammonia rates under similar conditions. We also find that ion-induced nucleation involves IO_3^- and the sequential addition of HIO_3 and that it proceeds at the kinetic limit below $+10^\circ\text{C}$. In contrast, neutral nucleation involves the repeated sequential addition of iodous acid (HIO_2) followed by HIO_3 , showing that HIO_2 plays a key stabilizing role. Freshly formed particles are composed almost entirely of HIO_3 , which drives rapid particle growth at the kinetic limit. Our measurements indicate that iodine oxoacid particle formation can compete with sulfuric acid in pristine regions of the atmosphere.

New particle formation plays an important role in radiative forcing of the climate. If particles survive to larger sizes, they influence climate directly, by scattering light, and indirectly, by producing more than half of all cloud condensation nuclei (CCN) (1). However, new

particle formation and aerosol–cloud interactions remain relatively poorly understood and constitute major uncertainties in determining Earth's equilibrium climate sensitivity with climate models (2). So far, only a few vapors that can form new particles under atmospheric conditions have been identified: sulfuric acid

(3–7), methanesulfonic acid (3, 8), iodine species (9–11), highly oxygenated organic molecules (HOMs) (12), and, more recently, nitric acid (13). Under warm conditions or low vapor concentrations, acidic molecular clusters further require base vapors such as ammonia (6, 13, 14) or dimethylamine (15) to stabilize them against evaporation. Ions can play a comparable role in stabilizing nucleating acidic (6) or biogenic (12) particles.

Marine new particle formation is especially important, as the ocean is vast, and marine clouds are highly sensitive to CCN because their concentrations are low. Marine clouds are radiatively important because they have a high infrared emission and albedo in contrast with the dark ocean surface. Marine new particle formation has thus been a focus for aerosol–climate interactions and feedbacks for many years (16), mostly concerning dimethylsulfide and its oxidation products (3, 8, 16). Although nucleation of iodine oxides was first studied almost 20 years ago (9, 10), iodine particle formation is presently considered to have limited global significance (17) and remains relatively poorly understood.

The ocean surface is a major source of atmospheric iodine; hypoidous acid (HOI) and molecular iodine (I_2) are emitted by the reaction of gaseous ozone with aqueous iodide (I^-) (18). Typical daytime emissions from the tropical Atlantic Ocean are 7×10^7 HOI molecules $\text{cm}^{-2} \text{s}^{-1}$ and 7×10^6 I_2 molecules $\text{cm}^{-2} \text{s}^{-1}$ (18), leading to daytime mixing ratios in the marine boundary layer of ~ 1 part per trillion by volume (pptv) HOI and 0.1 pptv iodine atoms (19). Land surfaces (vegetation and soils) emit comparable iodine fluxes as iodomethane (CH_3I), producing boundary layer mixing ratios of ~ 0.5 pptv and free tropospheric levels of ~ 0.1 pptv (20). Iodine compounds have been found at a variety of sites, including coastal regions (9, 10), Arctic sea ice (11, 21), the marine boundary layer (22), the lower (23) and upper free troposphere (24), and the stratosphere (25).

More recently, iodic acid (HIO_3) has been shown to drive coastal marine new particle formation at Mace Head, Ireland (11), and

¹Institute for Atmospheric and Earth System Research/Physics, Faculty of Science, University of Helsinki, 00014 Helsinki, Finland. ²Center for Atmospheric Particle Studies, Carnegie Mellon University, Pittsburgh, PA 15213, USA. ³Department of Chemistry and Cooperative Institute for Research in the Environmental Sciences, University of Colorado Boulder, Boulder, CO 80309, USA. ⁴Faculty of Physics, University of Vienna, 1090 Vienna, Austria. ⁵Aerosol Physics Laboratory, Physics Unit, Faculty of Engineering and Natural Sciences, Tampere University, 33014 Tampere, Finland. ⁶Institute for Atmospheric and Environmental Sciences, Goethe University Frankfurt, 60438 Frankfurt am Main, Germany. ⁷Department of Applied Physics, University of Eastern Finland, 70211 Kuopio, Finland. ⁸Laboratory of Atmospheric Chemistry, Paul Scherrer Institute, CH-5232 Villigen, Switzerland. ⁹CERN, the European Organization for Nuclear Research, CH-1211 Geneva 23, Switzerland. ¹⁰Division of Chemistry and Chemical Engineering, California Institute of Technology, Pasadena, CA 91125, USA. ¹¹CENTRA and Faculdade de Ciências da Universidade de Lisboa, 1749-016 Lisboa, Portugal. ¹²Leibniz Institute for Tropospheric Research, 04318 Leipzig, Germany. ¹³Institute of Meteorology and Climate Research, Karlsruhe Institute of Technology, 76344 Eggenstein-Leopoldshafen, Germany. ¹⁴Joint International Research Laboratory of Atmospheric and Earth System Sciences, School of Atmospheric Sciences, Nanjing University, Nanjing 210023, China. ¹⁵Jiangsu Provincial Collaborative Innovation Center of Climate Change, Nanjing 210023, China. ¹⁶Helsinki Institute of Physics, University of Helsinki, 00014 Helsinki, Finland. ¹⁷Institute of Ion Physics and Applied Physics, University of Innsbruck, 6020 Innsbruck, Austria. ¹⁸Ionicon Analytik Ges.m.b.H., 6020 Innsbruck, Austria. ¹⁹Institute of Physics, University of Tartu, 50411 Tartu, Estonia. ²⁰School of Civil and Environmental Engineering, Pusan National University, Busan 46241, Republic of Korea. ²¹Aerodyne Research, Inc., Billerica, MA 01821, USA. ²²P.N. Lebedev Physical Institute of the Russian Academy of Sciences, 119991 Moscow, Russia. ²³Finnish Meteorological Institute, 00560 Helsinki, Finland. ²⁴Department of Atmospheric and Oceanic Sciences, University of Colorado, Boulder, CO 80309, USA. ²⁵School of Earth and Environment, University of Leeds, Leeds LS2 9JT, UK. ²⁶Department of Atmospheric Chemistry and Climate, Institute of Physical Chemistry Rocasolano, CSIC, 28006 Madrid, Spain. ²⁷Institute of Chemistry, Eötvös University, H-1117 Budapest, Hungary. ²⁸Institute of Physics, Johannes Gutenberg University Mainz, 55128 Mainz, Germany. ²⁹Institute Infante Dom Luiz, University of Beira Interior, 6201-001 Covilhã, Portugal. ³⁰Aerosol and Haze Laboratory, Beijing Advanced Innovation Center for Soft Matter Science and Engineering, Beijing University of Chemical Technology, Beijing 100029, China. ³¹Department of Chemistry, University of Helsinki, University of Helsinki, 00014 Helsinki, Finland. ³²Department of Chemical Engineering, Carnegie Mellon University, Pittsburgh, PA 15213, USA. ³³Department of Engineering and Public Policy, Carnegie Mellon University, Pittsburgh, PA 15213, USA. ³⁴Department of Engineering and Public Policy, Carnegie Mellon University, Pittsburgh, PA 15213, USA.

*Corresponding author. Email: xucheng.he@helsinki.fi (X.-C.H.); jasper.kirkby@cern.ch (J.Ki.); mikko.sipila@helsinki.fi (M.Sip.)

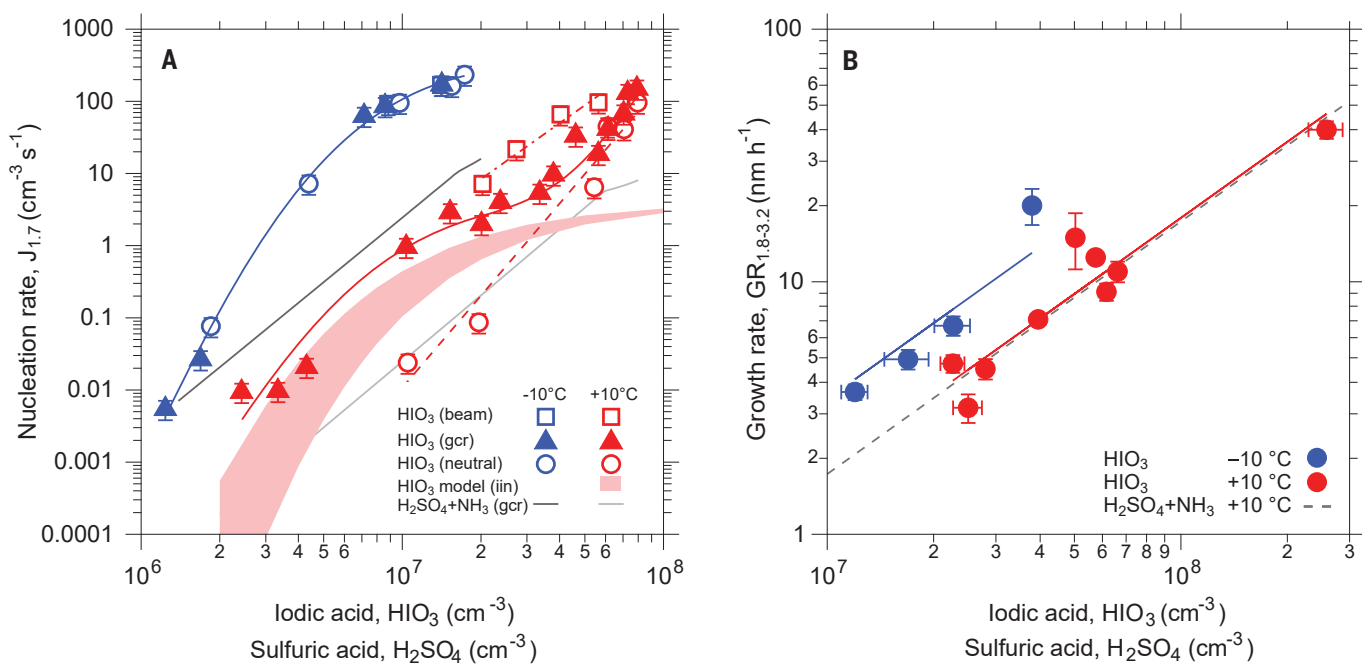


Fig. 1. Nucleation and growth rates versus iodine acid concentration.

(A) Nucleation rates at 1.7 nm diameter versus iodine acid concentration at +10°C (red symbols and curves) and -10°C (blue symbols and curves). Hollow circles show the nucleation rates for neutral conditions, J_n ; solid triangles for gcr conditions, J_{gcr} ; and hollow squares for beam conditions, J_{beam} . To guide the eye, the measurements are connected by approximate curves. The red band shows a kinetic model prediction for HIO_3 ion-induced nucleation, J_{lin} ($= J_{gcr} - J_n$), at +10°C (see supplementary materials for further details). The lower and upper limits correspond, respectively, to zero and two H_2O molecules per iodine atom in the cluster. For comparison, the gcr nucleation

rates measured for sulfuric acid with 100 pptv ammonia are shown at +10°C (light gray curve) and -10°C (dark gray curve) (14). (B) Mean growth rates of particles (neutral, gcr, and beam conditions) between 1.8 and 3.2 nm diameter versus HIO_3 concentration at +10°C (filled red circles) and -10°C (filled blue circles). For comparison, the dashed gray line shows the growth rates of $\text{H}_2\text{SO}_4\text{-NH}_3$ particles measured at +10°C (30). The bars in both panels represent $\pm 1\sigma$ measurement errors. The experimental conditions are 36 to 44 ppbv O_3 , 34 to 73% RH, 0.4 to 168 pptv I_2 , and an I atom production rate of 4.4×10^4 to $1.5 \times 10^7 \text{ cm}^{-3} \text{ s}^{-1}$. An overall systematic scale error on the HIO_3 concentration of -33% or +50% is not shown on the data points.

intense iodine particle formation has been reported along China's coast (26). So far, however, controlled laboratory experiments under atmospheric conditions are lacking, and so atmospheric observations of HIO_3 cannot be connected with predicted particle formation and growth rates. A mechanism for HIO_3 nucleation has been identified (11), but the ion-induced (charged) and neutral (uncharged) clusters were unseparated and may involve different iodine compounds. Furthermore, iodine oxides (I_xO_y) are presently considered to be the major species responsible for the growth and composition of iodine particles (9, 10, 27), although, once again, experimental measurements under atmospheric conditions are lacking.

Nucleation and growth rates

Here we report iodine new particle formation experiments performed under marine boundary layer conditions in the CERN CLOUD (Cosmics Leaving Outdoor Droplets) chamber (see supplementary methods) between September 2017 and November 2019. The experiments were conducted at +10° and -10°C, at 34 to 73% relative humidity (RH), and 20 to 46 parts per billion by volume (ppbv) ozone. We intro-

duced molecular iodine from an evaporator (0.4 to 168 pptv; median $\text{I}_2 = 6.4$ pptv) into the chamber.

The formation pathways of iodine oxoacids from iodine precursor vapors are not well understood, although computational studies assume that HO_x radicals are required to produce HIO_3 (28, 29). We tested this hypothesis by using green light (528 nm) alone to photolyze I_2 into iodine atoms. At full intensity, CLOUD's green light source photolyzes iodine vapor at a rate of $7 \times 10^{-3} \text{ s}^{-1}$, although most experiments were carried out at relative intensities of 10 to 20%. Because green light cannot photolyze O_3 , it gives rise to negligible HO_x . Nevertheless, we found that iodine atoms are rapidly oxidized in the presence of water vapor and ozone to produce both HIO_3 and iodous acid (HIO_2) (fig. S1). Iodine oxoacids can form from hydrated iodine atoms and iodine oxide radicals reacting with ozone, and they can also form from hydrolysis of I_xO_y (27). Under our experimental conditions, photolysis of I_2 typically produces $2 \times 10^5 \text{ I atoms cm}^{-3} \text{ s}^{-1}$ and ~ 1 pptv iodine monoxide (IO) radicals. The full range of conditions probed includes IO concentrations found in the open ocean marine boundary layer and

remote free troposphere (18, 19, 23, 24) (table S1). Notably, at constant actinic flux, HIO_3 increases linearly with iodine concentration, whereas HIO_2 increases as the square root (fig. S2). We speculate that iodine oxoacids form at CLOUD either from iodine radicals (e.g., $\text{I} + \text{H}_2\text{O} + \text{O}_3 \rightarrow \text{HIO}_3 + \text{OH}$) or the initial I_xO_y intermediates (e.g., $\text{I}_2\text{O}_2 + \text{H}_2\text{O} \rightarrow \text{HIO}_2 + \text{HOI}$). Because ozone and water vapor are found throughout the troposphere, our findings imply that molecular iodine will produce iodine oxoacids even under cloudy daylight conditions with negligible ultraviolet irradiation.

We show in Fig. 1A our measured nucleation rates at 1.7 nm, $J_{1.7}$, versus the HIO_3 concentration at +10° and -10°C and under three ionization conditions: neutral, J_n (ions eliminated from the chamber by a 20 kV m^{-1} electric field); galactic cosmic ray, J_{gcr} (boundary layer ion pair concentrations of $\sim 700 \text{ cm}^{-3}$); and beam enhanced, J_{beam} (ion pair concentrations of $\sim 2500 \text{ cm}^{-3}$, comparable to the upper free troposphere). The measurements were performed at contaminant ammonia levels near 3 pptv. The nucleation rates show a strong dependency on HIO_3 concentration, charge, and temperature. There is a large ion enhancement of the nucleation rate at +10°C,

whereas J_{ger} and J_{n} are comparable at -10°C . The nucleation rate increases rapidly as the temperature falls from $+10^{\circ}$ to -10°C . For comparison, we include in Fig. 1A our previous measurements of J_{ger} at 1.7 nm for sulfuric acid (H_2SO_4) with 100 pptv ammonia (NH_3) (14), which show that the nucleation rate of iodine oxoacids exceeds that of $\text{H}_2\text{SO}_4\text{-NH}_3$ at the same acid concentrations.

In Fig. 1B we show the dependence on HIO_3 concentration of the particle growth rates between 1.8 and 3.2 nm at $+10^{\circ}$ and -10°C . The growth rates of iodine oxoacid particles at $+10^{\circ}\text{C}$ are identical to our measurements for $\text{H}_2\text{SO}_4\text{-NH}_3$ particles between $+5^{\circ}$ and $+20^{\circ}\text{C}$ at the same acid concentrations (30). The close agreement implies that the iodine oxoacid particles are growing at the dipole-dipole enhanced kinetic limit for HIO_3 , with negligible evaporation at $+10^{\circ}\text{C}$ or below. The measurements further indicate that HIO_3 dominates the growth of iodine particles in this size range and above (because the Kelvin barrier falls with increasing size). This behavior is in marked contrast with previous studies that considered iodine oxides to be responsible for growth (10, 27). At -10°C , the growth rate of HIO_3 particles increases by a factor of 2. This faster growth exceeds the kinetic limit for the arrival rate of HIO_3 monomers onto the particles and is attributed to additional growth from HIO_3 molecular clusters—similar to the situation for sulfuric acid-dimethylamine particles (31)—which provide a large pool of condensable material that is “hidden” from the HIO_3 monomer measurement.

Our nucleation and growth rate measurements (Fig. 1) indicate that HIO_3 concentrations above $\sim 3 \times 10^6 \text{ cm}^{-3}$ and $1 \times 10^7 \text{ cm}^{-3}$ lead to rapid new particle formation at -10° and $+10^{\circ}\text{C}$, respectively. The survival probability of particles at low acid concentrations depends exponentially on the ratio of growth rate to condensation sink (in the atmosphere) or wall loss rate (in a chamber). For CLOUD, the wall loss rate of sulfuric acid vapor is $2.2 \times 10^{-3} \text{ s}^{-1}$ (30), which is comparable to the condensation sink in the pristine continental boundary layer. In clean marine regions of the boundary layer or in the upper free troposphere, the condensation sink is often as low as 10^{-4} to 10^{-5} s^{-1} . In such regions, even lower HIO_3 concentrations will lead to sustained new particle formation and subsequent growth rates of a few tenths of a nanometer per hour. Under such conditions of extremely low HIO_3 concentrations and condensation sinks, it is likely that ions will be important to stabilize the embryonic clusters against evaporation, i.e., ion-induced nucleation will be the dominant mechanism.

Particle formation mechanisms

In Fig. 2 we show mass defect plots of negatively charged clusters (Fig. 2A) and neutral

clusters (Fig. 2B) containing up to five iodine atoms, measured during nucleation events. The event in Fig. 2A is continued in fig. S3, up to clusters containing 12 iodine atoms. Figure S4 shows all identified peaks of the event in Fig. 2B, before summing over water molecules and charger ions as displayed in Fig. 2B. Further details of the charged and neutral clusters and their signal strengths are provided in table S2.

For ion-induced nucleation (Fig. 2A), we observe a sequence of negatively charged iodine clusters of the form $(\text{HIO}_3)_{0-1}(\text{I}_2\text{O}_5)_n\text{IO}_3^-$, involving sequential addition of HIO_3 fol-

lowed by rapid dehydration of $\text{HIO}_3\text{-HIO}_3$ pairs in the cluster to form I_2O_5 , as previously observed at Mace Head (11). We find that no nucleation occurs for positively charged iodine clusters (fig. S5). This is clearly seen from the negative and positive charged particle spectra in fig. S6; nucleation and growth only take place for negative particles. Almost all the negative particles have been neutralized by charge recombination before they reach 3 nm, and they continue to grow as mainly neutral particles. A schematic representation of the mechanism for ion-induced iodic acid nucleation,

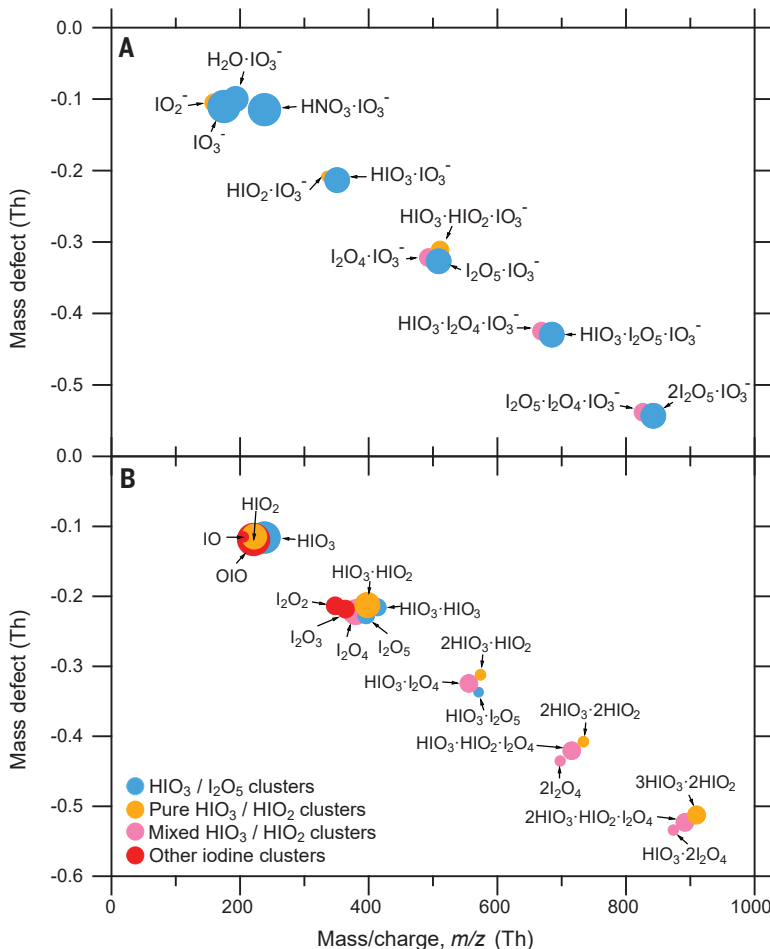


Fig. 2. Charged and neutral mass defect plots during nucleation events. Cluster mass defect (difference from integer mass) versus mass-to-charge ratio [m/z , in thomson (Th) units] of (A) negatively charged and (B) neutral clusters containing up to five iodine atoms, measured during nucleation events. The experimental conditions are (A) 36 ppbv O_3 , 40% RH, $+10^{\circ}\text{C}$, 168 pptv I_2 , and $1.5 \times 10^7 \text{ I atoms cm}^{-3} \text{ s}^{-1}$ and (B) 46 ppbv O_3 , 43% RH, $+10^{\circ}\text{C}$, 49 pptv I_2 , and $2.4 \times 10^5 \text{ I atoms cm}^{-3} \text{ s}^{-1}$. The event shown in (A) is continued in fig. S3 up to clusters containing 12 iodine atoms. To simplify (B), water molecules and nitrate charger ions are ignored (fig. S4 shows the same event where they are included). Charged clusters are measured with the API-TOF(-) (atmospheric pressure interface-time-of-flight mass spectrometer operating in negative ion mode) and neutral clusters with the nitrate-CIMS (chemical ionization mass spectrometer; preceded by an ion filter). We find that no nucleation takes place for positively charged clusters (figs. S5 and S6). Blue circles indicate clusters containing only HIO_3 and I_2O_5 . Orange circles indicate clusters containing only HIO_3 and HIO_2 . Pink circles indicate clusters containing HIO_3 , HIO_2 , I_2O_5 , and I_2O_4 . Red circles indicate other iodine-containing neutral clusters. The size of the circles indicates signal strength on a logarithmic scale. Further details of the clusters and their signal strengths are provided in table S2.

as interpreted from the mass defect plot (Fig. 2A), is provided in Fig. 3A.

Nucleation of neutral iodine oxoacid particles, however, proceeds by a different mechanism (Fig. 2B). We find that neutral $\text{HIO}_3\text{-I}_2\text{O}_5$ clusters are relatively weakly bound at these temperatures (no clusters of this type are seen above $\text{HIO}_3\text{-I}_2\text{O}_5$). During neutral nucleation, we observe repeated sequential addition of HIO_2 followed by HIO_3 . The nucleating cluster sequences are shown schematically in Fig. 3B. A certain fraction of $\text{HIO}_3\text{-HIO}_2$ pairs in the cluster dehydrate to form iodine tetroxide (I_2O_4) (Fig. 3C). The comparable intensities of the three sequences shown in Fig. 3C indicate that the formation rate of I_2O_4 in the neutral clusters is comparable to the monomer collision rate (few 10^{-3} s^{-1}). In contrast, the strict conversion of $\text{HIO}_3\text{-HIO}_3$ pairs during ion-induced nucleation (Fig. 3A) shows that the formation rate of I_2O_5 in the charged clusters is much faster than the monomer collision rate (few 10^{-2} s^{-1}).

Our measurements show that HIO_2 plays a key role in stabilizing neutral HIO_3 clusters. To assess this observation, we used quantum chemistry calculations to compute the formation free energy of several molecular dimers involving HIO_3 (table S3 and fig. S7). The most strongly bound dimer is $\text{HIO}_3\text{-HIO}_2$ ($-12.9 \text{ kcal mol}^{-1}$). On the other hand, the $\text{HIO}_3\text{-HIO}_3$ ($-7.7 \text{ kcal mol}^{-1}$) and $\text{HIO}_3\text{-HOI}$ ($-1.6 \text{ kcal mol}^{-1}$) dimers are both much less

stable. These calculations argue in favor of the dominant $\text{HIO}_3\text{-HIO}_2$ dimer shown in the 1 \rightarrow 2 iodine step in Fig. 3B and not $\text{HIO}_3\text{-HIO}_3$ at the current experimental conditions. Our measurements and quantum chemical calculations suggest that HIO_2 stabilizes neutral HIO_3 clusters with a 1:1 stoichiometry similar to that seen for ammonia stabilization of embryonic H_2SO_4 clusters (6). For completeness, we note that, for neutral nucleation, the direct addition of I_2O_4 molecules from gas phase I_2O_4 , which we measure at concentrations of $\sim 1\%$ of HIO_3 (table S2), cannot be excluded. We also note that HIO_3 shows very weak affinity for pairing with a base ($\text{HIO}_3\text{-NH}_3$ is $-5.0 \text{ kcal mol}^{-1}$). Once the neutral particles exceed a critical size, they can continue to grow by condensation of HIO_3 alone (most of the particles in Fig. 1B are neutralized), and so growth is no longer limited by the lower concentrations of HIO_2 .

Ion-induced nucleation rate

To investigate ion-induced nucleation further, we measured the collision rate coefficients, k_{i+1} , for each step in the process, $\text{N}_i^- + \text{HIO}_3 \rightarrow \text{N}_{i+1}^-$, where N_i^- represents a negatively charged cluster containing i iodine atoms [see (32) and the supplementary materials for further details]. The rate coefficients measured between neutral HIO_3 monomers and charged clusters containing up to 11 iodine

atoms are shown in Fig. 4A. Within measurement errors, we find the same HIO_3 rate coefficient for each charged iodic cluster from the dimer to 11-mer, with a mean value [$1.72 \pm 0.26 \text{ (stat.)} + 0.24/-0.21 \text{ (syst.)} \times 10^{-9} \text{ cm}^3 \text{ s}^{-1}$ (1σ uncertainties)]. For comparison, we show the theoretical expectations for the rate coefficients for charged HIO_3 clusters from average dipole orientation theory (ADO, red curve) (33) and its extensions: hard-sphere average dipole orientation theory (HSA, green curve) and surface charge capture theory (SCC, blue curve) (34). The latter theory, SCC, agrees closely with our measurements. We show in Fig. 4B the enhancement factors for charged versus neutral rate coefficients (ratios of the CLOUD measurements divided by the neutral rate coefficients, ignoring dipole enhancement). The enhancement during ion-induced nucleation, which averages 6.3, rapidly shepherds newly formed particles through the smallest size range where they are highly mobile and most vulnerable to scavenging loss, and it contributes to the faster particle formation rate.

Our measurements of the individual collision rate coefficients for charged clusters containing up to 11 iodine atoms (Fig. 4A)—and their good agreement with theoretical expectations—show that ion-induced iodic acid nucleation proceeds at the kinetic limit and therefore is strictly a barrierless process rather than nucleation. Substantial evaporation of any cluster in this range would lead to a telltale higher apparent rate coefficient for the previous cluster. We have confirmed kinetic formation of charged clusters in two further ways. (i) We have used a kinetic model to calculate the ion-induced component of $J_{\text{gr}} (= J_{\text{in}} + J_{\text{n}})$ at $+10^\circ\text{C}$ (see supplementary materials for details) and find it is consistent with our experimental measurements (Fig. 1A). (ii) We have calculated the reaction free energies and evaporation rates for several molecular clusters containing an IO_3^- ion (table S4). Our calculations show that extremely low evaporation rates are expected for charged iodic acid clusters. They also indicate that the $\text{HIO}_3\text{-HIO}_3\text{-IO}_3^-$ cluster is much less stable than $\text{I}_2\text{O}_5\text{-IO}_3^-$, supporting the sequence observed experimentally in the first steps of Fig. 3A. The HIO_3 collision rate measurements in Fig. 4A confirm that ion-induced nucleation is indeed due to the sequential addition of HIO_3 monomers and not, for example, to mixed accretion of HIO_3 and I_2O_5 molecules.

Particle composition

The measurements presented in Fig. 1B provide strong evidence that HIO_3 drives the growth of iodic particles above 1.8 nm. However, we have seen that additional iodine compounds play important roles during nucleation: HIO_2 for neutral nucleation, and the formation of iodine oxides— I_2O_5 and I_2O_4 —in the charged and neutral clusters, respectively (Fig. 2).

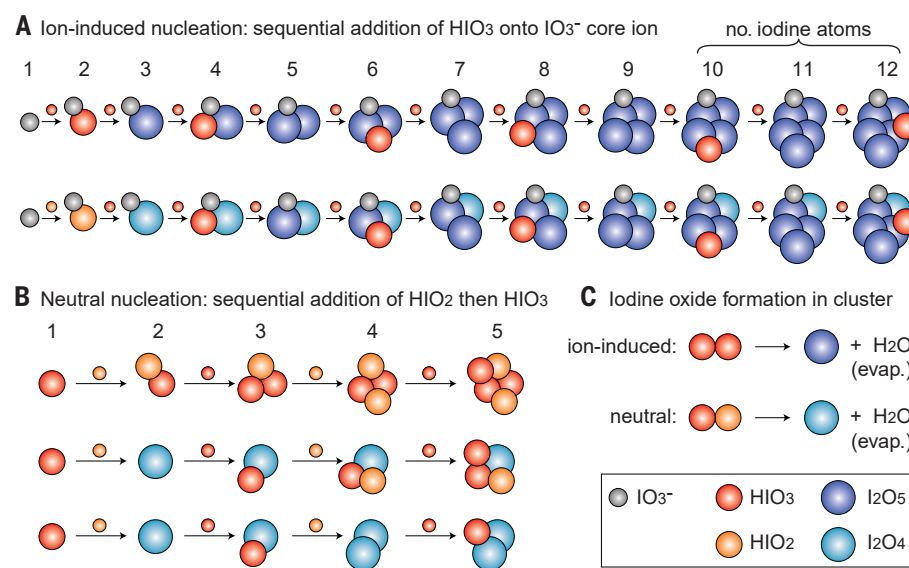


Fig. 3. Nucleation mechanisms for iodine oxoacid clusters. Schematic representations of the nucleation mechanisms for (A) ion-induced (charged) and (B) neutral (uncharged) iodine oxoacid clusters, interpreted from the mass defect plots. Ion-induced nucleation involves condensation of iodic acid (HIO_3) alone onto an IO_3^- ion, whereas neutral nucleation involves repeated stepwise condensation of iodous acid (HIO_2) followed by iodic acid. Iodine oxide formation takes place in the clusters, as shown in (C), involving evaporation (evap.) of a water molecule. Pairs of HIO_3 molecules always dehydrate to form I_2O_5 in charged clusters (A). However, HIO_3 molecules do not form I_2O_5 in neutral clusters, but some may combine with HIO_2 and dehydrate to form I_2O_4 (B). The relative intensities of the final neutral clusters in (B) are $(\text{HIO}_3)_3(\text{HIO}_2)_2:(\text{HIO}_3)_2\text{HIO}_2\text{-I}_2\text{O}_4:\text{HIO}_3\text{-}(\text{I}_2\text{O}_4)_2 = 0.38:0.46:0.16$, indicating that the formation rate of I_2O_4 in the neutral clusters is comparable to the monomer collision rate.

Fig. 4. Collision rate coefficients for ion-induced iodic acid nucleation.

(A) Collision rate (reaction rate) coefficients measured between neutral HIO_3 monomers and charged clusters containing up to 11 iodine atoms. The experimental conditions are 20 to 41 ppbv O_3 , 34 to 44% RH, +10°C, 0.4 to 3.5 pptv I_2 , and 0.44×10^5 to 3.2×10^5 $\text{I atoms cm}^{-3} \text{ s}^{-1}$. The gray triangles are calculated from the 50% appearance times of eight experiments with 0.76×10^7 to $2.0 \times 10^7 \text{ cm}^{-3}$ HIO_3 . The red circles are the final experimental values after applying corrections from a kinetic model. The experimental points are horizontally shifted from integers to avoid overlaps. The solid curves show theoretical expectations for the charged collision rate coefficients from average dipole orientation theory (ADO, red curve) (36), hard-sphere average dipole orientation theory (HSA, green curve) (37), and surface charge capture theory (SCC, blue curve) (37). The expected collision rate coefficients between neutral monomers and neutral clusters, ignoring dipole-dipole interactions, are shown by the dashed black curve. **(B)** Measured enhancement factors for charged versus neutral collision rate coefficients (ratios of the corrected CLOUD measurements divided by the neutral collision rate coefficients). The black dotted line is the ratio of the SCC value to the neutral kinetic theory value. For both panels, the hollow markers show the weighted mean values from the trimer to 11-mer, with $\pm 1\sigma$ errors indicating statistical without (inner caps) and with systematic errors (outer).

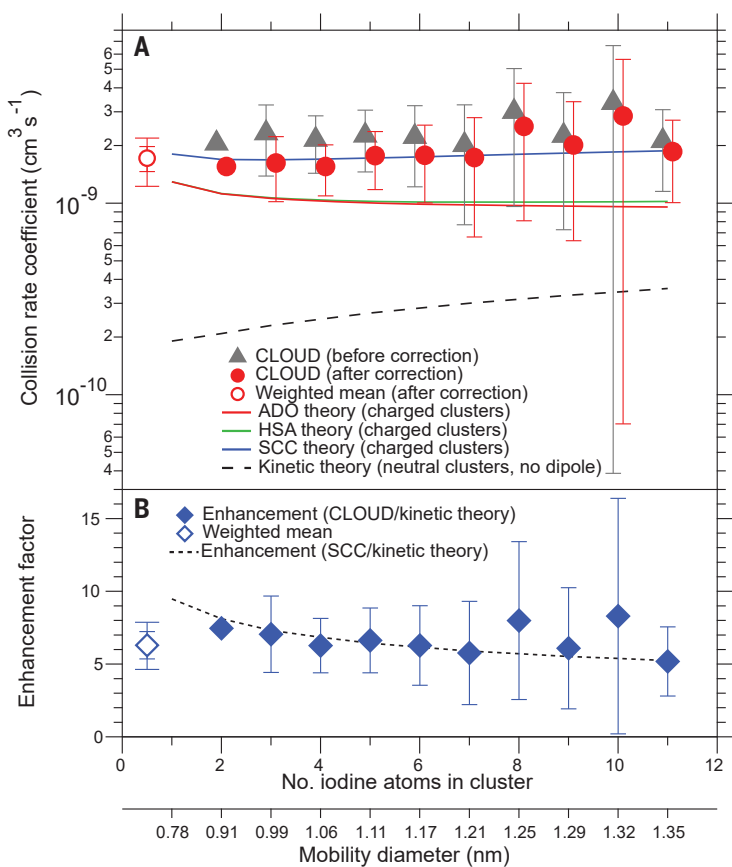
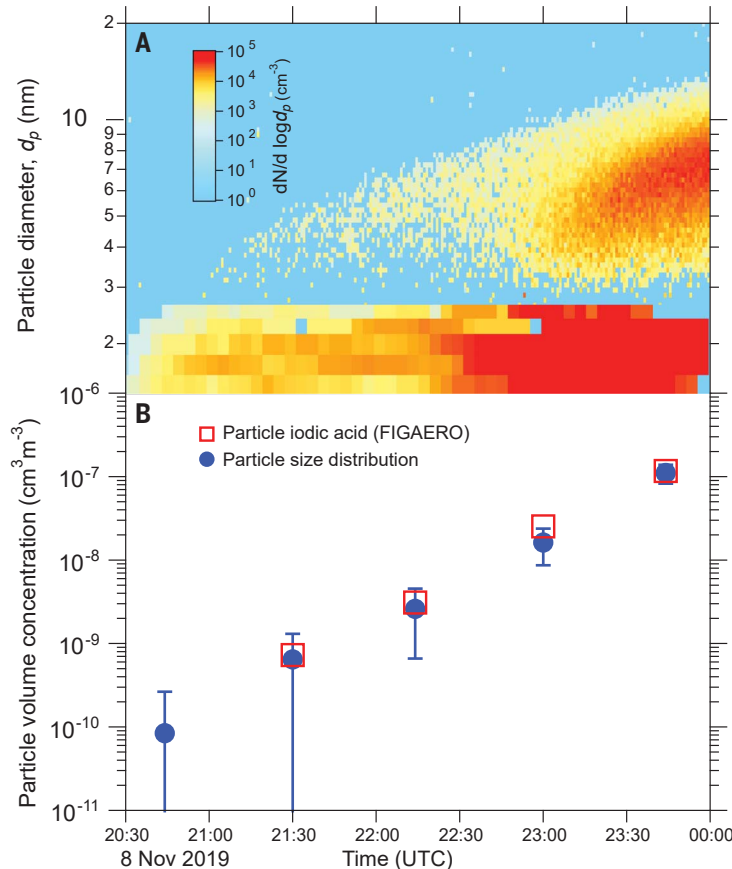


Fig. 5. Evolution of particle size and chemical composition during iodic oxoacids nucleation. **(A)** Evolution of the particle size distribution measured by the particle size magnifier (PSM; smaller than 2.5 nm) and nano-scanning mobility particle sizer (nano-SMPS; larger than ~4 nm). The experimental conditions are 40 ppbv O_3 , 40% RH, +10°C, 8 pptv I_2 , 2.9×10^5 to $5.3 \times 10^5 \text{ I atoms cm}^{-3} \text{ s}^{-1}$, and 3.1×10^7 to $7.1 \times 10^7 \text{ cm}^{-3}$ HIO_3 . The event is started by switching on green illumination (528 nm), and HIO_3 is increased toward the end. **(B)** Evolution of the particle volume concentration derived from (i) the particle size distribution (blue circles) and (ii) the HIO_3 volume for particles collected and analyzed with the FIGAERO (hollow red squares). Particle concentrations in the size range between 2.5 and 4 nm are obtained by interpolation between the PSM and nano-SMPS distributions and are verified by measurements of the total number concentrations above a 2.5-nm threshold of the PSM. The FIGAERO collects particles on a Teflon filter for 30 min and then evaporates the sample with a controlled temperature ramp over the next 15 min at the inlet of the mass spectrometer. The FIGAERO data points are centered on the 30-min collection interval. The bars indicate $\pm 1\sigma$ total errors. The FIGAERO mass spectrum shows that HIO_3 dominates the particle composition (80% mass fraction). This is independently confirmed by the close agreement between the volume concentrations measured by the particle sizers and by the FIGAERO.



To address the question of the extent to which these other iodine species contribute to particle growth at larger sizes, we have directly measured the composition of freshly nucleated iodide particles in the size range up to ~ 10 nm with a soft-ionization Br⁻-FIGAERO (filter inlet for gases and aerosols) mass spectrometer. The majority (90%) of particles between 3 and 10 nm are neutral (fig. S6). The FIGAERO collects particles on a Teflon filter for 30 min and then evaporates the sample with a controlled temperature ramp over the next 15 min at the inlet of a mass spectrometer. The mass spectrometer thereby measures the deposited mass of each chemical constituent of the particles and produces an individual thermogram of its volatility (evaporation temperature).

In Fig. 5A we show the evolution of particle size during a nucleation experiment. Particle sizes <2.5 nm are measured by a PSM (particle size magnifier), and those >4 nm are measured by a nano-SMPM (scanning mobility particle sizer). In Fig. 5B we show the evolution of total particle volume derived from these measurements (blue circles). We also show in Fig. 5B the evolution of total HIO₃ volume concentration in the particle phase, measured by the FIGAERO. The mass spectrum is dominated by the single channel, HIO₃ (78% of the total mass, excluding water), with the rest being primarily I₂. We found very little HIO₂ in the particle phase, owing to its low concentration. The mass spectrum shows that the freshly formed particles are composed almost entirely of HIO₃, and not I₂O₄₋₅ as previously thought (9–11). This conclusion is independently confirmed by the close agreement seen in Fig. 5B between the volume concentrations measured by the particle sizers and by the direct measurements of particulate HIO₃ with the FIGAERO. We have confirmed, by conducting laboratory calibrations, that the evaporated HIO₃ resulted from iodide acid in the particle phase, and not by thermal decomposition of other iodine compounds. We nebulized iodide acid particles and then collected and analyzed them with the FIGAERO using the same procedures as for our experiments at CLOUD (see supplementary materials for details). The FIGAERO thermograms for the nebulized samples agree well with those obtained at CLOUD (fig. S8).

Climate implications

Sulfuric acid–ammonia nucleation is known to be important in relatively pristine environments such as the free troposphere (14) or the Antarctic coastal region (35). We show here that the nucleation rate of iodide oxoacids exceeds H₂SO₄–NH₃ at the same acid concentrations. In pristine, cooler regions of the atmosphere, HIO₃ concentrations above $\sim 10^6$ cm⁻³ will lead to copious new particle formation and sustained growth at a few times 0.1 nanometer

per hour. The question then arises: Are there pristine regions of the atmosphere where the concentrations of HIO₃ are comparable to or exceed sulfuric acid, or else ammonia is insufficient? For such regions, HIO₃ could be the dominant source of new particles.

Our global boundary layer measurements of HIO₃ at 10 sites are shown in figs. S9 and S10. The conditions for abundant iodide new particle formation and rapid growth are frequently reached at mid-latitude coastal sites with marine algae, such as Mace Head and Helsinki, and at coastal polar sites such as Villum and Ny-Ålesund in the Arctic, or Neumayer in the Antarctic. Although measurements over the remote ocean are sparse, frequent new particle formation over the high Arctic pack ice has recently been reported, driven by HIO₃ with little contribution from sulfuric acid (36).

The implications for the future are notable. Global iodide emissions have increased three-fold over the past 70 years and may continue to increase in the future as sea ice becomes thinner (37) and surface ozone increases (18). Any resultant increase of iodide CCN in the Arctic region could increase longwave radiative forcing from clouds and provide a positive feedback mechanism that accelerates the loss of sea ice. Iodide is also widespread in the free troposphere (23, 24), where low temperatures, low condensation sinks, and high ion production rates from galactic cosmic rays favor iodide particle formation. Indeed, particulate iodide (IO₃⁻) has recently been observed near the tropopause at iodide mixing ratios of ~ 0.1 to 0.5 pptv, and IO₃⁻ is the main iodide reservoir in the stratosphere (25) (further discussion is provided in the supplementary materials).

Our study shows that iodide acid, HIO₃, is the major iodide species driving both nucleation and growth of iodide oxoacid particles in the boundary layer and remains as the dominant constituent in the particulate phase. We have further shown that iodide acid, HIO₂, plays a key role in neutral nucleation by stabilizing HIO₃ clusters against evaporation, but it is not important for particle growth at larger sizes. The efficacy of iodide oxoacids to form new particles exceeds that of the H₂SO₄–NH₃ system at the same acid concentrations. Although atmospheric measurements remain limited, they are nevertheless sufficient to demonstrate the ubiquity of HIO₃ and its potential to compete with sulfuric acid–(ammonia) particle formation in pristine regions of the atmosphere such as marine coasts, the Arctic boundary layer, or the upper free troposphere.

REFERENCES AND NOTES

1. H. Gordon *et al.*, *J. Geophys. Res.* **122**, 8739–8760 (2017).
2. G. A. Meehl *et al.*, *Sci. Adv.* **6**, eaab1981 (2020).
3. S. M. Kreidenweis, J. H. Seinfeld, *Atmos. Environ.* **22**, 283–296 (1988).
4. P. H. McMurry *et al.*, *J. Geophys. Res.* **110**, D22S02 (2005).
5. C. Kuang, P. H. McMurry, A. V. McCormick, F. L. Eisele, *J. Geophys. Res.* **113**, D10209 (2008).
6. J. Kirkby *et al.*, *Nature* **476**, 429–433 (2011).
7. M. Kulmala *et al.*, *Science* **339**, 943–946 (2013).
8. M. L. Dawson *et al.*, *Proc. Natl. Acad. Sci. U.S.A.* **109**, 18719–18724 (2012).
9. T. Hoffmann, C. D. O'Dowd, J. H. Seinfeld, *Geophys. Res. Lett.* **28**, 1949–1952 (2001).
10. C. D. O'Dowd *et al.*, *Nature* **417**, 632–636 (2002).
11. M. Sipilä *et al.*, *Nature* **537**, 532–534 (2016).
12. J. Kirkby *et al.*, *Nature* **533**, 521–526 (2016).
13. M. Wang *et al.*, *Nature* **581**, 184–189 (2020).
14. E. M. Dunne *et al.*, *Science* **354**, 1119–1124 (2016).
15. J. Almeida *et al.*, *Nature* **502**, 359–363 (2013).
16. R. J. Charlson, J. E. Lovelock, M. O. Andreae, S. G. Warren, *Nature* **326**, 655–661 (1987).
17. T. M. Sherwen *et al.*, *Geophys. Res. Lett.* **43**, 10012–10019 (2016).
18. L. J. Carpenter *et al.*, *Nat. Geosci.* **6**, 108–111 (2013).
19. A. S. Mahajan *et al.*, *Atmos. Chem. Phys.* **10**, 4611–4624 (2010).
20. B. C. Sive *et al.*, *Geophys. Res. Lett.* **34**, L17808 (2007).
21. J. D. Allan *et al.*, *Atmos. Chem. Phys.* **15**, 5599–5609 (2015).
22. C. Prados-Roman *et al.*, *Atmos. Chem. Phys.* **15**, 583–593 (2015).
23. B. Dix *et al.*, *Proc. Natl. Acad. Sci. U.S.A.* **110**, 2035–2040 (2013).
24. R. Volkamer *et al.*, *Atmos. Meas. Tech.* **8**, 2121–2148 (2015).
25. T. K. Koenig *et al.*, *Proc. Natl. Acad. Sci. U.S.A.* **117**, 1860–1866 (2020).
26. H. Yu *et al.*, *Atmos. Chem. Phys.* **19**, 4025–4039 (2019).
27. J. C. Gómez Martín *et al.*, *Nat. Commun.* **11**, 4521 (2020).
28. E. Drougas, A. M. Kosmas, *J. Phys. Chem. A* **109**, 3887–3892 (2005).
29. J. M. C. Plane, D. M. Joseph, B. J. Allan, S. H. Ashworth, J. S. Francisco, *J. Phys. Chem. A* **110**, 93–100 (2006).
30. D. Stolzenburg *et al.*, *Atmos. Chem. Phys.* **20**, 7359–7372 (2020).
31. K. Lehtipalo *et al.*, *Nat. Commun.* **7**, 11594 (2016).
32. X.-C. He *et al.*, *Aerosol Sci. Technol.* **55**, 231–242 (2021).
33. T. Su, M. T. Bowers, *J. Chem. Phys.* **58**, 3027–3037 (1973).
34. G. Kummerlöwe, M. K. Beyer, *Int. J. Mass Spectrom.* **244**, 84–90 (2005).
35. T. Jokinen *et al.*, *Sci. Adv.* **4**, eaat9744 (2018).
36. A. Baccarini *et al.*, *Nat. Commun.* **11**, 4924 (2020).
37. C. A. Cuevas *et al.*, *Nat. Commun.* **9**, 1452 (2018).
38. X.-C. He *et al.*, Role of iodide oxoacids in atmospheric aerosol nucleation: data resources, Version 1, Zenodo (2021); <http://doi.org/10.5281/zenodo.4299441>.

ACKNOWLEDGMENTS

Funding: We thank the European Organization for Nuclear Research (CERN) for supporting CLOUD with important technical and financial resources and for providing a particle beam from the CERN Proton Synchrotron. This research has received support from the Academy of Finland (projects 316114, 307331, 310682, 266388, 3282290, 306853, 296628, 229574, 333397, 326948, and 1325656); the European Research Council (projects 692891, 616075, 764991, 316662, 742206, and 714621); CSC – Finnish IT center; the EC Seventh Framework Programme and the EU H2020 programme Marie Skłodowska Curie ITN “CLOUD-TRAIN” (316662) and “CLOUD-MOTION” (764991); Austrian Science Fund (FWF) (J3951-N36 and P27295-N20); the Swiss National Science Foundation (20F02_159851, 200021_169090, 200020_172602, and 20F02_172622); the U.S. National Science Foundation (grants AGS1447056, AGS1439551, AGS1801574, AGS1620530, AGS1801897, AGS153128, AGS1649147, AGS1801280, AGS1602086, and AGS1801329); MSCA H2020 COFUND-FP-CERN-2014 fellowship (665779); German Federal Ministry of Education and Research: CLOUD-16 (01LK1601A); Portuguese Foundation for Science and Technology (CERN/FIS-COM/0014/2017); Academy of Finland Centre of Excellence in Atmospheric Sciences (grant 272041); European Regional Development Fund (project MOBTT42); Jiangsu Collaborative Innovation Center for Climate Change; Yangtze River Delta Atmosphere and Earth System Science National Observation and Research Station; Estonian Research Council (project PRG714); Hungarian National Research, Development and Innovation Office (K116788 and K132254); NASA Graduate Fellowship (NASA-NNX16AP36H); and ACTRIS 2 TNA H2020 OCTAVE (654109). We are also grateful for all the people who have contributed to the field measurements around the world.

Author contributions: X.-C.H., M.K., R.V., J.Ki., and M.Sip. planned the experiments. X.-C.H., Y.J.T., L.D., M.W., H.F., D.S., M.Sim., A.Kü., J.S., B.R., S.I., M.R., S.Scho., R.B., D.S.W., T.K.K., S.A., A.A., K.K., S.B., L.C., D.C., B.C., A.Dia., J.Du., I.E.H., R.C.F., L.G.C., M.G., M.H., V.H., H.J., J.Ka., D.K., C.K., W.K., J.E.K., A.Kv., T.L., H.L., C.P.L., K.L., M.L., Z.L., V.M., H.E.M., G.M., R.M., R.L.M., B.M., O.M., T.M., A.O., T.P., J.P., M.P., W.S., S.Schul., B.S., G.S., Y.S., A.T., M.V.-P., A.C.W., S.K.W., W.N., P.M.W., Y.Wu., A.Y., Y.Wang, M.Z.-W., Q.Z., J.C., M.K., U.B., R.V., J.Ki., and M.Sip. prepared the CLOUD

facility or measuring instruments. X.-C.H., Y.J.T., L.D., M.W., H.F., D.S., M.Sim., J.S., B.R., M.R., R.B., D.S.W., T.K.K., T.J., N.S., L.J.B., F.A., A.B., F.B., B.B., S.B., D.C., R.C., A.Din., J.Du., L.G.C., M.G., M.H., V.H., H.J., D.K., C.K., J.E.K., H.L., C.P.L., M.L., Z.L., H.E.M., G.M., R.M., R.L.M., B.M., T.M., J.P., A.R., I.S., S.Schul., B.S., G.S., C.T., A.T., R.C.T., O.V., M.V.-P., A.C.W., S.K.W., W.N., Y.Wu., M.X., C.Y., Q.Y., A.Y., Y.Wang., M.Z.-W., R.V., and J.Ki. collected the data. X.-C.H., Y.J.T., L.D., M.W., H.F., D.S., M.Sim., J.S., B.R., R.C.F., D.K., C.K., W.K., S.K.W., P.M.W., P.Z., T.K., R.V., J.Ki., and D.R.W. analyzed the data. J.Ki. and X.-C.H. wrote the manuscript with

contributions from R.V., Y.J.T., M.W., H.F., T.K.K., M.K., T.K., N.M.D., D.R.W., and M.Sip. X.-C.H., Y.J.T., L.D., M.W., H.F., D.S., B.R., S.I., M.R., S.Scho., R.B., T.K.K., N.S., A.B., A.Din., J.Do., J.Du., I.E.H., A.H., H.J., J.Ka., J.E.K., H.L., C.P.L., K.L., R.L.M., B.M., O.M., T.P., A.S.-L., I.S., P.Z., J.C., U.B., M.K., V.-M.K., T.K., N.M.D., R.V., J.Ki., D.R.W., and M.Sip. commented on and edited the manuscript. **Competing interests:** The authors declare no competing interests. **Data and materials availability:** Data for all figures in the main text and supplementary materials are available at the Zenodo repository (38).

SUPPLEMENTARY MATERIALS

science.sciencemag.org/content/371/6529/589/suppl/DC1
 Materials and Methods
 Supplementary Text
 Figs. S1 to S10
 Tables S1 to S4
 References (39–81)

27 July 2020; accepted 6 January 2021
 10.1126/science.abe0298

Role of iodine oxoacids in atmospheric aerosol nucleation

Xu-Cheng He, Yee Jun Tham, Lubna Dada, Mingyi Wang, Henning Finkenzeller, Dominik Stolzenburg, Siddharth Iyer, Mario Simon, Andreas Kürten, Jiali Shen, Birte Rörup, Matti Rissanen, Siegfried Schobesberger, Rima Baalbaki, Dongyu S. Wang, Theodore K. Koenig, Tuija Jokinen, Nina Sarnela, Lisa J. Beck, João Almeida, Stavros Amanatidis, António Amorim, Farnoush Ataei, Andrea Baccarini, Barbara Bertozi, Federico Bianchi, Sophia Brilke, Lucia Caudillo, Dexian Chen, Randall Chiu, Biwu Chu, António Dias, Aijun Ding, Josef Dommen, Jonathan Duplissy, Imad El Haddad, Loïc Gonzalez Carracedo, Manuel Granzin, Armin Hansel, Martin Heinritzi, Victoria Hofbauer, Heikki Junninen, Juha Kangasluoma, Deniz Kemppainen, Changhyuk Kim, Weimeng Kong, Jordan E. Krechmer, Aleksander Kvashin, Totti Laitinen, Houssni Lamkaddam, Chuan Ping Lee, Katrianne Lehtipalo, Markus Leiminger, Zijun Li, Vladimir Makhmutov, Hanna E. Manninen, Guillaume Marie, Ruby Marten, Serge Mathot, Roy L. Mauldin, Bernhard Mentler, Ottmar Möhler, Tatjana Müller, Wei Nie, Antti Onnela, Tuukka Petäjä, Joschka Pfeifer, Maxim Philippov, Ananth Ranjithkumar, Alfonso Saiz-Lopez, Imre Salma, Wiebke Scholz, Simone Schüchmann, Benjamin Schulze, Gerhard Steiner, Yuri Stozhkov, Christian Tauber, António Tomé, Roseline C. Thakur, Olli Väistönen, Miguel Vazquez-Pufleau, Andrea C. Wagner, Yonghong Wang, Stefan K. Weber, Paul M. Winkler, Yusheng Wu, Mao Xiao, Chao Yan, Qing Ye, Arttu Yli-Sirniö, Marcel Zauner-Wieczorek, Qiaozhi Zha, Putian Zhou, Richard C. Flagan, Joachim Curtius, Urs Baltensperger, Markku Kulmala, Veli-Matti Kerminen, Theo Kurtén, Neil M. Donahue, Rainer Volkamer, Jasper Kirkby, Douglas R. Worsnop and Mikko Sipilä

Science 371 (6529), 589-595.
DOI: 10.1126/science.abe0298

Faster than expected

Iodine species are one of only a handful of atmospheric vapors known to make new aerosol particles, which play a central role in controlling the radiative forcing of climate. He *et al.* report experimental evidence from the CERN Cosmics Leaving Outdoor Droplets, or CLOUD, chamber demonstrating that iodic acid and iodous acid rapidly form new particles and can compete with sulfuric acid in pristine regions.

Science, this issue p. 589

ARTICLE TOOLS

<http://science.sciencemag.org/content/371/6529/589>

SUPPLEMENTARY MATERIALS

<http://science.sciencemag.org/content/suppl/2021/02/03/371.6529.589.DC1>

REFERENCES

This article cites 78 articles, 11 of which you can access for free
<http://science.sciencemag.org/content/371/6529/589#BIBL>

PERMISSIONS

<http://www.sciencemag.org/help/reprints-and-permissions>

Use of this article is subject to the [Terms of Service](#)

Science (print ISSN 0036-8075; online ISSN 1095-9203) is published by the American Association for the Advancement of Science, 1200 New York Avenue NW, Washington, DC 20005. The title *Science* is a registered trademark of AAAS.

Copyright © 2021 The Authors, some rights reserved; exclusive licensee American Association for the Advancement of Science. No claim to original U.S. Government Works